Kinetic analysis of mechanochemical reaction between zinc oxide and gamma ferric oxide based on the impact energy and collision frequency of particles

Kinetic analysis of mechanochemical reaction between zinc oxide and gamma ferric oxide based on the impact energy and collision frequency of particles

Fumie Hirosawa, Tomohiro Iwasaki*, Masashi Iwata

Department of Chemical Engineering, Osaka Prefecture University, Sakai, Osaka 599-8531, Japan

*Corresponding author:

Tomohiro Iwasaki

E-mail: iwasaki@chemeng.osakafu-u.ac.jp

Postal address: 1-1 Gakuen-cho, Naka-ku, Sakai, Osaka, 599-8531, Japan

Tel: +81–72–254–9307, Fax: +81–72–254–9911

Abstract

A new method for analyzing the rate of mechanochemical reactions using the kinetic energy and collision frequency of the reactive particles has been proposed based on the theoretical analysis of thermal chemical reactions. The rate constant of a mechanochemical reaction to form zinc ferrite through high-energy ball milling of a mixture of zinc oxide and gamma ferric oxide (maghemite) as the model mechanochemical reaction system was experimentally determined at several revolution speeds in a planetary mill. Based on the kinetic theory of molecules in a thermal chemical reaction, the kinetic energy of the particles was numerically determined from the velocity distribution of particles, which was obtained by a discrete element method (DEM) simulation of the particle and ball motion. The collision frequency of particles was also calculated and related to the kinetic energy according to the collision theory for molecules. Finally, the reaction rate constant was expressed as a pseudo-Arrhenius equation including a frequency factor and an energy factor as an alternative to the Boltzmann factor. Our method for analyzing the rate of mechanochemical reactions can contribute to precise control of their reaction rates.

Keywords

Mechanochemical reaction, Kinetic energy, Collision frequency, Reaction rate constant, Velocity distribution, Discrete element method (DEM)

1. Introduction

Mechanochemical reactions are induced by mechanical energy derived from collisions of reactive particles [1, 2], and have been widely used to synthesize various functional nanoparticles [3–8]. Planetary ball mills are often employed to conduct mechanochemical reactions. In the planetary mill, the reactive particles violently collide with each other, causing the mechanochemical reaction to progress. The degree of progress of the reaction can be affected by not only the kinetic energy of the particles, but also by the number of the collisions per unit time. Accordingly, the reaction rate depends strongly on the kinetic energy and collision frequency of the reactive particles. This may be very similar to the way in which the rates of thermal chemical reactions in gas, liquid, and solid phases are governed by the kinetic energy and collision frequency of molecules.

Based on statistical thermodynamics, the reaction rate of thermal chemical reactions has been expressed using the Arrhenius equation, which consists of the Boltzmann factor and a frequency factor [9−12], which reflect the kinetic energy and the collision frequency of molecules, respectively, and determine the reaction rate. The kinetic energy of the molecules is expressed in terms of $k_B T$, where k_B is the Boltzmann constant and T is the temperature [13]. Generally, the $k_B T$ term is referred to as thermal energy and represents the energy level of the system at a given temperature. $k_B T$ depends on the velocity distribution of the molecules, which is related to the thermal motion. The collision frequency of the molecules is determined according to collision theory in thermal chemical reactions [13, 14]. In contrast, in mechanochemical reactions, the kinetic energy and collision frequency of particles, which greatly affect the reaction rate, have been analyzed experimentally [15–19]. In order to precisely control the rate of mechanochemical reactions, theoretical investigations of their kinetics are needed.

In this paper, not only an experimental approach, but also a theoretical one is employed to analyze the rate of a mechanochemical reaction. The kinetic energy and the collision frequency of the particles were determined by computing the motion of the particles. In addition, mechanochemical reaction experiments were performed, and the reaction rate was determined. A chemical reaction in which zinc ferrite ($ZnFe_2O_4$) was formed mechanochemically from zinc oxide (ZnO) and maghemite (γ-Fe_2O_3) in a high-energy planetary mill was employed as the model mechanochemical reaction system. Based on the theoretical analysis of thermal chemical reactions, we propose a method for the semi-theoretical analysis of the rate of mechanochemical reactions using kinetic energy and collision frequency.

2. Methods

2.1. Calculations for the determination of the kinetic energy and collision frequency of the particles

To obtain the kinetic energy and collision frequency of the particles, the behavior of the particles and balls in a planetary mill under dry conditions was simulated using the discrete element method (DEM), which is a reliable method for the simulation of solid particle behavior [20–24]. The DEM simulation method in this work was based on that proposed by Tsuji et al. [25], and the parameters of the simulation were defined in accordance with the experimental settings of the planetary mill discussed later, and are listed in Table 1 [26–34].

In the simulation, zirconia balls were used as the grinding balls, and the particles were assumed to form granules composed of reactant (ZnO and γ-Fe_2O_3) nanoparticles,

product ($ZnFe_2O_4$) nanoparticles, and voids. For the granule particles, the following assumptions were made: (i) the nanoparticles in the granule particles as well as on their surfaces were distributed homogeneously with the voids, and (ii) the void fraction was 0.26, corresponding to the hexagonal closest packing. The molar fractions of the different nanoparticles in the granule particles changed depending on the progress of the reaction, as shown in Fig. 1a. The density of the granule particles was approximated as the arithmetic mean of the true densities of the nanoparticles including the voids, regardless of the progress of the reaction, because the true densities of the components were similar: being 5606 kg/m^3 (ZnO) [27], 5240 kg/m^3 (Fe_2O_3) [28], and 5325 kg/m^3 ($ZnFe_2O_4$) [29]. The Young's modulus of the granule particles was regarded as one-tenth of the arithmetic mean of those of the components [30–34]. Furthermore, the restitution coefficient of zirconia-zirconia collisions (i.e., ball-ball/wall collisions) has been measured [35], and those of zirconia-granule (i.e., ball/wall-granule particle collisions) and granule-granule collisions were also experimentally determined using the balls and walls covered with a sufficient amount of granule particles. The zirconia-zirconia, zirconia-granule, and granule-granule friction coefficients were determined based on the experimentally measured critical rotational speeds of a tumbling pot [36].

The impact energy $\boldsymbol{E}_\mathrm{p}$ of a granule particle is defined by Eq. (1) as the mechanical energy consumed for the progress of the mechanochemical reaction.

$$\boldsymbol{E}_\mathrm{p} = \frac{1}{2}\boldsymbol{m}_\mathrm{p}\boldsymbol{v}_\mathrm{p}^{\,2} \tag{1}$$

where $\boldsymbol{v}_\mathrm{p}$ is the relative velocity of a granule particle at a collision and $\boldsymbol{m}_\mathrm{p}$ is the reduced mass of the granule particle and the subject of the collision.

The collision frequency of ZnO nanoparticles with Fe_2O_3 nanoparticles on the

surface of the granule particles affects the rate of the mechanochemical reaction ZnO + $Fe_2O_3 \rightarrow ZnFe_2O_4$. In order to obtain the collision frequency of the nanoparticles in the simulation, pure ZnO, Fe_2O_3, and $ZnFe_2O_4$ spheres composed of ZnO, Fe_2O_3 and $ZnFe_2O_4$ nanoparticles, respectively, and voids, were assumed, as shown in Fig. 1b. Assuming that the spheres had the same properties (such as diameter, true density, void fraction, Young's modulus, and Poisson's ratio) as the granule particles, we simulated the behaviors of the spheres rather than those of the granule particles. Additionally, the number ratio (which is the same as the true volume ratio) of ZnO, Fe_2O_3, and $ZnFe_2O_4$ spheres in the mill pot were determined using the true volume ratios of ZnO, Fe_2O_3, and $ZnFe_2O_4$ nanoparticles in the granule particles, respectively. The collision frequency $\boldsymbol{Z}_{nano}$ between ZnO and Fe_2O_3 nanoparticles is related to that of the spheres, $\boldsymbol{Z}_{sp}$, as expressed by Eq. (2) (see Appendix).

$$\boldsymbol{Z}_{nano} = \frac{\boldsymbol{W}_{total}^{\ 2}}{\boldsymbol{V}_{total}^{\ 2}\rho_{ZnO}\rho_{Fe2O3}}\boldsymbol{Z}_{sp} \tag{2}$$

where ρ_{ZnO} and ρ_{Fe2O3} are the true densities of the ZnO and Fe_2O_3 nanoparticles, respectively, and $\boldsymbol{W}_{total}$ and $\boldsymbol{V}_{total}$ are the total molar mass and total molar true volume of the granule particles at a conversion of $\boldsymbol{x}$, respectively. In this system, $\boldsymbol{W}_{total}^2/(\boldsymbol{V}_{total}^2\rho_{ZnO}\rho_{Fe2O3})$ was approximately constant (0.97) regardless of $\boldsymbol{x}$, due to the similar densities of the particles.

The conversion $\boldsymbol{x}$ is defined as the ratio of the number of reacted ZnO spheres at time $\boldsymbol{t}$ to the number of all-ZnO spheres in the mill pot prior to milling, as shown in Fig. 1c, which illustrates the definition of conversion using $\boldsymbol{x}$ = 0 and 0.5 as examples. The number ratio of the spheres varies with the progress of the reaction.

Therefore, the collision frequency $\boldsymbol{Z}_{sp}$ between ZnO spheres and Fe_2O_3 spheres at a given $\boldsymbol{x}$ was obtained using the number of collisions α_{sp} between ZnO spheres and Fe_2O_3 spheres for the time period $\boldsymbol{t}$.

$$\boldsymbol{Z}_{sp} = \alpha_{sp}/\boldsymbol{t} \quad (3)$$

In the study, $\boldsymbol{E}_p$ and $\boldsymbol{Z}_{sp}$ were calculated at different mill pot revolution speeds $\boldsymbol{N}$ and conversions $\boldsymbol{x}$.

2.2. Experiment for the determination of the reaction rate constant

The ZnO nanoparticles and the γ-Fe_2O_3 nanoparticles used in this work were supplied by Sakai Chemical Industry and Wako Pure Chemical Industries, respectively. According to the suppliers, the average diameter and purity of ZnO and γ-Fe_2O_3 nanoparticles were approximately 20 nm and >96% (ZnO) and 20–40 nm and 97.0% (γ-Fe_2O_3), respectively. In the experiments to determine the reaction rate constant, 2.5 g of the starting materials were weighed in a molar ratio of 1.0, which coincided with the stoichiometric ratio of $ZnFe_2O_4$. A planetary mill (Pulverisette-7, Fritsch) with a pair of zirconia pots with inner volumes of 45 mL, each containing 180 zirconia (YTZ) balls 5 mm in diameter, was used to prepare the $ZnFe_2O_4$ nanoparticles. The ball-to-particle mass ratio (BPR) was 28.3, which was the same as the simulation condition. The powder mixture was placed in each mill pot and ground in air at room temperature. The revolution speed of the mill pot and the duration of the process were determined considering the applicable conditions of the proposed model. Our model can be applied to conditions that the mechanochemical reaction smoothly proceeds due to sufficient amounts of unreacted particles. Thus, the milling conditions of excessively prolonged times and/or higher

revolution speeds should be avoided because the mechanism of reaction process may significantly differ from our model due to severe aggregation of particles. Therefore, the revolution speed and duration were varied within the ranges of 5.0–10.0 s^{-1} and 0–4.32×10^4 s, respectively. Revolution was suspended for 5 min after every 10 min of milling to avoid excess temperature increase inside the mill pots during processing.

The phase evolution of the samples during milling was evaluated using a powder X-ray diffractometer (XRD; RINT-1500, Rigaku, CuKα radiation, 40 kV, 80 mA). The morphology of the samples was observed with a field emission scanning electron microscope (FE-SEM; JSM-6700F, JEOL, 18.0 kV). The ZnO and γ-Fe_2O_3 nanoparticles before milling were also observed with FE-SEM as shown in Fig. 2, confirming their diameter mentioned earlier. Moreover, in order to determine the conversion $\boldsymbol{x}$, the content of unreacted ZnO in the samples was quantified using the following leaching method [37]: 0.2 g of the ground powder was soaked in 43 g of 0.1 mol/L H_2SO_4 solution for 3 h at room temperature. A preliminary leaching test confirmed that 0.2 g of ZnO could be completely dissolved within 3 h under the same leaching conditions. The undissolved particles in the solution were separated by centrifugation. Finally, the zinc concentration of the leaching solution was measured using inductively coupled plasma analysis (ICP; SPS7800, Hitachi High-Technologies), and the conversion $\boldsymbol{x}$ of ZnO was determined.

$$\boldsymbol{x} = 1 - (\boldsymbol{n_t}/\boldsymbol{n_0}) \tag{4}$$

where $\boldsymbol{n_0}$ and $\boldsymbol{n_t}$ are the molar amounts of ZnO in the powder mixture before and after milling for time $\boldsymbol{t}$, respectively.

3. Results and discussion

3.1. Velocity distribution and kinetic energy of the granule particles

In the analysis of thermal chemical reactions, the velocity distribution of molecules is expressed using the Maxwell distribution, and results from the random thermal motion of the molecules [13]. The motion of the granule particles in the planetary mill is also random in the circumferential-direction due to the orbital motion of the mill pot, and the velocities of granule particles can be described using a distribution. In order to analyze the velocity distribution of the granule particles, the distribution was assumed to be expressed by Eq. (5), which is a formula similar to the Maxwell distribution in cylindrical coordinates ($\boldsymbol{r}$, θ, $\boldsymbol{z}$).

$$\boldsymbol{f}(\boldsymbol{v}_r, \boldsymbol{v}_\theta, \boldsymbol{v}_z)\mathrm{d}\boldsymbol{v}_r\mathrm{d}\boldsymbol{v}_\theta\mathrm{d}\boldsymbol{v}_z = \boldsymbol{C}_\mathrm{p}\boldsymbol{v}_r \exp\left\{-\beta_\mathrm{p}\frac{\boldsymbol{m}_\mathrm{p}}{2}(\boldsymbol{v}_r^{\,2} + \boldsymbol{v}_\theta^{\,2} + \boldsymbol{v}_z^{\,2})\right\}\mathrm{d}\boldsymbol{v}_r\mathrm{d}\boldsymbol{v}_\theta\mathrm{d}\boldsymbol{v}_z \tag{5}$$

where $\boldsymbol{v}_r$, $\boldsymbol{v}_\theta$, and $\boldsymbol{v}_z$ are the translational velocities of a granule particle in the $\boldsymbol{r}$-, θ-, and $\boldsymbol{z}$-directions, respectively, and β_p and $\boldsymbol{C}_\mathrm{p}$ are the coefficients. Based on the Maxwell distribution, $1/\beta_\mathrm{p}$ can be assumed as the kinetic energy of granule particles, which represents the level of mechanical energy. $\boldsymbol{f}(\boldsymbol{v}_r, \boldsymbol{v}_\theta, \boldsymbol{v}_z)$ is the probability function, $(1/2)\boldsymbol{m}_\mathrm{p}(\boldsymbol{v}_r^2 + \boldsymbol{v}_\theta^2 + \boldsymbol{v}_z^2)$ is the kinetic energy of a granule particle, and $\boldsymbol{v}_r\mathrm{d}\boldsymbol{v}_r\mathrm{d}\boldsymbol{v}_\theta\mathrm{d}\boldsymbol{v}_z$ is the infinitesimal volume. Moreover, the translational velocity $\boldsymbol{v}$ of a granule particle is given by Eq. (6).

$$\boldsymbol{v} = \sqrt{\boldsymbol{v}_r^{\,2} + \boldsymbol{v}_\theta^{\,2} + \boldsymbol{v}_z^{\,2}} \tag{6}$$

In the planetary mill, the distribution of the velocity $\boldsymbol{v}_r$ of the granule particles in the $\boldsymbol{r}$-

direction may be higher than that of the velocity v_z in the z-direction, because the acceleration of the granule particles due to the planetary motion of the mill pot is rather high compared to the gravity acceleration. Thus, the infinitesimal volume $v_r dv_r dv_\theta dv_z$ of velocity is represented by a spheroidal shell of possible velocity vectors, expressed by $\eta\pi v^2 dv$, where η is the coefficient. Therefore, the translational velocity distribution of the granule particles can be rewritten as Eq. (7):

$$f(v)dv = C_{p2} v^2 \exp\left(-\beta_p \frac{m_p v^2}{2}\right) dv \tag{7}$$

where C_{p2} is the coefficient and is represented by Eq. (8), because the probability function must sum to 1 over the entire range of the velocity as Eq. (9).

$$C_{p2} = \sqrt{\frac{2}{\pi}(\beta_p m_p)^3} \tag{8}$$

$$\int_0^\infty f(v)dv = 1 \tag{9}$$

Therefore, similar to the determination of $k_B T$ in thermal chemical reactions, the kinetic energy of the granule particles representing the level of mechanical energy can be determined by applying Eq. (7) to the velocity distribution of the granule particles obtained by the simulation.

In order to estimate the kinetic energy of the granule particles, we defined an apparent translational velocity of the granule particles as the translational velocity of the granule particles having a kinetic energy equivalent to the impact energy. Fig. 3 shows the apparent translational velocity distribution of the granule particles. The velocity distribution of the granule particles varied greatly with even slight changes in N and

shifted to higher velocity with an increase in N. The observed changes were similar to those of the velocity distribution of molecules due to temperature in thermal chemical reactions [13]. Subsequently, Eq. (7) was applied to the velocity distributions, as shown in Fig. 3. The distribution curves obtained from the simulation had a tendency similar to Eq. (7). Fig. 4 shows the change in the value of $1/\beta_p$ in Eq. (7) with N. $1/\beta_p$ was proportional to N, which was similar to the fact that $k_B T$ is proportional to the temperature T in thermal chemical reactions. The results imply that $1/\beta_p$ could correspond to the level of mechanical energy contributing to the progress of the mechanochemical reaction.

3.2. Collision frequency of the spheres

According to the collision theory of molecules [13, 14], the collision frequency Z_{sp} of the spheres was assumed to be expressed by Eq. (10).

$$Z_{sp} = \pi(r_{sp,ZnO} + r_{sp,Fe2O3})^2 \left\langle v_{sp,rel} \right\rangle \Delta t V_p \frac{N_{sp0,ZnO} N_{sp0,Fe2O3}}{V_p^2} (1-x_{ZnO})(1-x_{Fe2O3})(1-\varepsilon_v)^2 \frac{1}{\Delta t} \quad (10)$$

where $r_{sp,ZnO}$ and $r_{sp,Fe2O3}$ are the radii of the ZnO and Fe_2O_3 spheres, respectively, and V_p is the volume of the mill pot. $N_{sp0,ZnO}$ and $N_{sp0,Fe2O3}$ are the initial numbers of ZnO and Fe_2O_3 spheres, respectively, and x_{ZnO} and x_{Fe2O3} are the conversions of the ZnO and Fe_2O_3 spheres, respectively. ε_v is the void fraction of a single sphere, and $\left\langle v_{sp,rel} \right\rangle$ is the average relative velocity of the spheres, which is given as Eq. (11) when the velocity distribution of the spheres is expressed by Eq. (7).

$$\left\langle v_{sp,rel} \right\rangle = \sqrt{2} \int_0^\infty v f(v) \mathrm{d}v = \frac{4}{\sqrt{\pi m_p}} \sqrt{1/\beta_p} \quad (11)$$

In this reaction system, the decrease in the number of ZnO spheres was the same as that in the number of Fe_2O_3 spheres, and the conversions of ZnO and Fe_2O_3 could be written in terms of the common conversion $\boldsymbol{x}$.

$$\boldsymbol{x}_{ZnO} = \boldsymbol{x}_{Fe2O3} = \boldsymbol{x} \tag{12}$$

Additionally, the radii of the ZnO and Fe_2O_3 spheres were the same in the simulation. Therefore, using Eqs. (10), (11), and (12), the collision frequency $\boldsymbol{Z}_{sp}$ between ZnO spheres and Fe_2O_3 spheres can be rewritten as Eq. (13) including $1/\beta_p$.

$$\boldsymbol{Z}_{sp} = \frac{16\pi \boldsymbol{r}_{sp,ZnO}{}^2 \boldsymbol{N}_{sp0,ZnO} \boldsymbol{N}_{sp0,Fe2O3} (1-\varepsilon_v)^2}{\boldsymbol{V}_p \sqrt{\pi \boldsymbol{m}_p}} \sqrt{1/\beta_p} (1-\boldsymbol{x})^2 \tag{13}$$

Fig. 5 shows the relationship between $\boldsymbol{Z}_{sp}$ and $(1-\boldsymbol{x})^2$ and that between $\boldsymbol{Z}_{sp}$ and $\sqrt{1/\beta_p}$, which were obtained from the simulation using different conversions $\boldsymbol{x}$ and revolution speeds $\boldsymbol{N}$. $\boldsymbol{Z}_{sp}$ was proportional to both $(1-\boldsymbol{x})^2$ and $\sqrt{1/\beta_p}$. As a result, the $\boldsymbol{Z}_{sp}$ value thus obtained was confirmed to be a function of $(1-\boldsymbol{x})^2$ and $\sqrt{1/\beta_p}$, as expressed by Eq. (13).

3.3. Reaction rate constant

Fig. 6 shows the XRD patterns of the samples milled for different durations at $\boldsymbol{N}$ = 10.0 s^{-1} as an example. Before milling, only the ZnO and γ-Fe_2O_3 phases were observed. After milling for 3.60×10^3 s, the peaks corresponding to the ZnO and γ-Fe_2O_3 phases were obviously weakened and broadened due to amorphization. Furthermore, after milling for 3.24×10^4 s, the samples were found to contain the $ZnFe_2O_4$ phase regardless of $\boldsymbol{N}$. The result confirmed that the reaction (ZnO + γ-Fe_2O_3 → $ZnFe_2O_4$) progressed

mechanochemically. However, small amounts of the reactive particles remained even in long durations at high revolutions because the particles tended to strongly aggregate under the conditions, suggesting that the mechanism of reaction process in the final stage changed from that in the initial and intermediate stages. On the other hand, as shown in Fig. 6, during the initial stage of the reaction, the phase transition from γ-Fe_2O_3 to α-Fe_2O_3 was identified, which was observed regardless of $\boldsymbol{N}$.

Fig. 7 shows the typical SEM image of the sample obtained after milling for 3.24×10^4 s at $\boldsymbol{N}$ = 10.0 s^{-1}. At the milling condition, the sample was almost composed of $ZnFe_2O_4$ as mentioned above and the primary particle diameter was approximately 50–100 nm, indicating the formation of $ZnFe_2O_4$ nanoparticles by the mechanochemical reaction.

Fig. 8 illustrates the conversion $\boldsymbol{x}$ of ZnO as a function of the milling time $\boldsymbol{t}$ at different $\boldsymbol{N}$ values. $\boldsymbol{x}$ increased with an increase in $\boldsymbol{t}$ and $\boldsymbol{N}$, since larger amounts of mechanical energy were applied to the reactive particles at longer $\boldsymbol{t}$ and higher $\boldsymbol{N}$. In order to obtain the rate of the mechanochemical reaction from the experimental data, the reaction rate $d\boldsymbol{x}/d\boldsymbol{t}$ was expressed in terms of the rate constant $\boldsymbol{k}$ of the overall reaction, i.e., ZnO + γ-Fe_2O_3 → $ZnFe_2O_4$, using Eq. (14) except for the final stage of the reaction process.

$$\frac{d\boldsymbol{x}}{d\boldsymbol{t}} = \boldsymbol{k}(1-\boldsymbol{x})^{\boldsymbol{p}} \tag{14}$$

where $\boldsymbol{p}$ is the experimental constant and was determined to be 1.4 in this system. Fig. 9 shows the change in the reaction rate constant $\boldsymbol{k}$ with $\boldsymbol{N}$. The reaction rate constant $\boldsymbol{k}$ increased with an increase in $\boldsymbol{N}$, i.e., with a higher level of mechanical energy. Furthermore, the revolution speed $\boldsymbol{N}$ at $\boldsymbol{k}$ = 0 may be the threshold of $\boldsymbol{N}$ at which the

reaction can occur.

3.4. Rate of the mechanochemical reaction

Based on the Arrhenius equation for thermal chemical reactions, the rate of mechanochemical reactions was assumed to be given by Eq. (15), which includes the collision frequency $\boldsymbol{Z}_{\mathrm{nano}}$ of the nanoparticles in the granule particles and the kinetic energy $1/\beta_{\mathrm{p}}$ of the granule particles, which represents the level of mechanical energy:

$$\boldsymbol{k} \propto \boldsymbol{Z}_{\mathrm{nano}} \exp\left(-\frac{\boldsymbol{E}_{\mathrm{pa}}}{1/\beta_{\mathrm{p}}} \right) \tag{15}$$

where $\boldsymbol{E}_{\mathrm{pa}}$ is the coefficient. The collision frequency $\boldsymbol{Z}_{\mathrm{nano}}$ of the nanoparticles is proportional to the collision frequency $\boldsymbol{Z}_{\mathrm{sp}}$ of the spheres. Furthermore, $\boldsymbol{Z}_{\mathrm{sp}}$ is also proportional to $\sqrt{1/\beta_{\mathrm{p}}}$ and $(1-\boldsymbol{x})^2$ as mentioned above. Therefore, Eq. (15) can be rewritten as Eq. (16) using a coefficient γ.

$$\boldsymbol{k} = \gamma \sqrt{1/\beta_{\mathrm{p}}} \exp\left(-\frac{\boldsymbol{E}_{\mathrm{pa}}}{1/\beta_{\mathrm{p}}} \right) \tag{16}$$

In order to demonstrate that the rate of the mechanochemical reaction can be expressed by Eq. (16), the experimentally determined values of $\boldsymbol{k}$ were semi-logarithmically plotted against the $(1/\beta_{\mathrm{p}})^{-1}$ values obtained from the DEM simulation. Fig. 10 shows the relationship between $\ln \boldsymbol{k}$ and $(1/\beta_{\mathrm{p}})^{-1}$. Eq. (16) approximated the correlation well, and the values of $\boldsymbol{E}_{\mathrm{pa}}$ and γ were determined to be 2.3×10^{-7} J and 0.35 $\mathrm{s^{-1}\cdot J^{-1/2}}$, respectively. The coefficient $\boldsymbol{E}_{\mathrm{pa}}$ might correspond to the threshold energy for the mechanochemical reaction. The results suggested that the reaction rate constant could be expressed as a

pseudo-Arrhenius equation including a frequency factor and an energy factor as an alternative to the Boltzmann factor.

4. Conclusion

The rate of the mechanochemical reaction to form $ZnFe_2O_4$ via high-energy ball milling of a mixture of ZnO and γ-Fe_2O_3 was analyzed based on the kinetic theories for thermal chemical reactions. The kinetic energy $1/\beta_p$ of the granule particles, which represents the level of mechanical energy contributing to progress of the mechanochemical reaction, was determined by the velocity distribution of the granule particles using the DEM simulation. The collision frequency was also obtained by DEM and expressed as a function of $1/\beta_p$. The reaction rate constant could be expressed in terms of the energy factor and frequency factor, similarly to the Arrhenius equation for thermal chemical reactions. The results suggest that this method of analyzing the rate of mechanochemical reactions could contribute to precise control of the reaction rate.

Nomenclature

$\boldsymbol{C}_p$	Coefficient [s^3/m^3]
$\boldsymbol{C}_{p2}$	Coefficient [s^3/m^3]
$\boldsymbol{E}_p$	Impact energy of a granule particle [J]
$\boldsymbol{E}_{pa}$	Coefficient [J]
$\boldsymbol{k}$	Reaction rate constant [s^{-1}]
$\boldsymbol{k}_B$	Boltzmann constant [J/K]
$\boldsymbol{M}_{Fe2O3}$	Molecular weight of Fe_2O_3 [kg/mol]

$M_{ZnFe2O4}$ Molecular weight of $ZnFe_2O_4$ [kg/mol]

M_{ZnO} Molecular weight of ZnO [kg/mol]

m_p Reduced mass of a granule particle and the subject of the collision [kg]

N Revolution speed of the mill pot [s^{-1}]

N_{all} Total number of granule particles in the mill pot [–]

N_{Fe2O3} Number of Fe_2O_3 spheres in the simulation [–]

$N_{sp0,Fe2O3}$ Initial number of Fe_2O_3 spheres [–]

$N_{sp0,ZnO}$ Initial number of ZnO spheres [–]

$N_{ZnFe2O4}$ Number of $ZnFe_2O_4$ spheres in the simulation [–]

N_{ZnO} Number of ZnO spheres in the simulation [–]

n_t Molar amount of ZnO in powder mixture after milling [mol]

n_0 Molar amount of ZnO in powder mixture before milling [mol]

p Experimental constant [–]

$r_{sp,Fe2O3}$ Radius of Fe_2O_3 sphere [m]

$r_{sp,ZnO}$ Radius of ZnO sphere [m]

T Temperature [K]

t Time [s]

V_{Fe2O3} True volume of Fe_2O_3 nanoparticles in a single granule particle [m^3]

V_g Volume of a single granule particle including voids [m^3]

V_p Volume of the mill pot [m^3]

V_{total} Total molar true volume of granule particles [m^3/mol]

$V_{ZnFe2O4}$ True volume of $ZnFe_2O_4$ nanoparticles in a single granule particle [m^3]

V_{ZnO} True volume of ZnO nanoparticles in a single granule particle [m^3]

v Translational velocity of a granule particle [m/s]

$\boldsymbol{v}_{\mathrm{p}}$ Relative velocity of a granule particle at a collision [m/s]

$\boldsymbol{v}_{\boldsymbol{r}}$ Translational velocity of a granule particle in $\boldsymbol{r}$-direction [m/s]

$\left\langle \boldsymbol{v}_{\mathrm{sp,rel}} \right\rangle$ Average relative velocity of spheres [m/s]

$\boldsymbol{v}_{\boldsymbol{z}}$ Translational velocity of a granule particle in $\boldsymbol{z}$-direction [m/s]

$\boldsymbol{v}_{\theta}$ Translational velocity of a granule particle in θ-direction [m/s]

$\boldsymbol{W}_{\mathrm{total}}$ Total molar mass of granule particles [kg/mol]

$\boldsymbol{x}$ Conversion [–]

$\boldsymbol{x}_{\mathrm{Fe2O3}}$ Conversion of Fe_2O_3 spheres [–]

$\boldsymbol{x}_{\mathrm{ZnO}}$ Conversion of ZnO spheres [–]

$\boldsymbol{Z}_{\mathrm{nano}}$ Collision frequency of ZnO nanoparticles and Fe_2O_3 nanoparticles [s^{-1}]

$\boldsymbol{Z}_{\mathrm{sp}}$ Collision frequency of ZnO spheres and Fe_2O_3 spheres [s^{-1}]

α_{sp} Number of collisions between ZnO spheres and Fe_2O_3 spheres [–]

β_{p} Coefficient [J^{-1}]

γ Coefficient [$s^{-1} \cdot J^{-1/2}$]

ε_{v} Void fraction [–]

η Coefficient [–]

$\bar{\rho}$ True density of a single granule particle [kg/m^3]

ρ_{Fe2O3} True density of a Fe_2O_3 nanoparticle [kg/m^3]

ρ_{ZnFe2O4} True density of a $ZnFe_2O_4$ nanoparticle [kg/m^3]

ρ_{ZnO} True density of a ZnO nanoparticle [kg/m^3]

ϕ_{Fe2O3} Volume fraction of Fe_2O_3 nanoparticles in a single granule particle with voids [–]

ϕ_{ZnFe2O4} Volume fraction of $ZnFe_2O_4$ nanoparticles in a single granule particle with voids [–]

ϕ_{ZnO} Volume fraction of ZnO nanoparticles in a single granule particle with voids [–]

Acknowledgement

This work was supported by JSPS Research Fellowships for Young Scientists, and JSPS KAKENHI Grant Number JP18J21860.

Appendix A. Collision frequencies of nanoparticles and spheres

Assuming that the ZnO, Fe_2O_3, and $ZnFe_2O_4$ nanoparticles are distributed homogeneously with voids in the granule particles, the collision frequency $\boldsymbol{Z}_{nano}$ between ZnO nanoparticles and Fe_2O_3 nanoparticles on the surfaces of the granule particles can be obtained theoretically as follows. The molar amounts of ZnO, Fe_2O_3, and $ZnFe_2O_4$ nanoparticles in a single granule particle at a conversion of $\boldsymbol{x}$ are represented by $\boldsymbol{n}_0(1-\boldsymbol{x})/\boldsymbol{N}_{all}$, $\boldsymbol{n}_0(1-\boldsymbol{x})/\boldsymbol{N}_{all}$, and $\boldsymbol{n}_0\boldsymbol{x}/\boldsymbol{N}_{all}$, respectively, where $\boldsymbol{n}_0$ is the molar amount of ZnO nanoparticles in the mill pot before milling and $\boldsymbol{N}_{all}$ is the total number of the granule particles in the mill pot. The true volumes $\boldsymbol{V}_{ZnO}$, $\boldsymbol{V}_{Fe2O3}$, and $\boldsymbol{V}_{ZnFe2O4}$ of ZnO, Fe_2O_3, and $ZnFe_2O_4$ nanoparticles in a single granule particle at $\boldsymbol{x}$ are expressed by Eqs. (A1), (A2) and (A3), respectively, using their molar amounts mentioned above, their molecular weights $\boldsymbol{M}_{ZnO}$, $\boldsymbol{M}_{Fe2O3}$, and $\boldsymbol{M}_{ZnFe2O4}$, and their true densities ρ_{ZnO}, ρ_{Fe2O3}, and $\rho_{ZnFe2O4}$.

$$\boldsymbol{V}_{ZnO} = \frac{\boldsymbol{n}_0}{\boldsymbol{N}_{all}}(1-\boldsymbol{x})\left(\frac{\boldsymbol{M}_{ZnO}}{\rho_{ZnO}}\right) \tag{A1}$$

$$\boldsymbol{V}_{Fe2O3} = \frac{\boldsymbol{n}_0}{\boldsymbol{N}_{all}}(1-\boldsymbol{x})\left(\frac{\boldsymbol{M}_{Fe2O3}}{\rho_{Fe2O3}}\right) \tag{A2}$$

$$\boldsymbol{V}_{\mathrm{ZnFe2O4}} = \frac{\boldsymbol{n}_0}{\boldsymbol{N}_{\mathrm{all}}} \boldsymbol{x} \left(\frac{\boldsymbol{M}_{\mathrm{ZnFe2O4}}}{\rho_{\mathrm{ZnFe2O4}}} \right) \tag{A3}$$

Thus, the volume $\boldsymbol{V}_{\mathrm{g}}$ (including voids) of a single granule particle is given by Eqs. (A4) and (A5) using the void fraction ε_{v} of a single granule particle.

$$\boldsymbol{V}_{\mathrm{g}} = \frac{\boldsymbol{V}_{\mathrm{ZnO}} + \boldsymbol{V}_{\mathrm{Fe2O3}} + \boldsymbol{V}_{\mathrm{ZnFe2O4}}}{1 - \varepsilon_{\mathrm{v}}} = \frac{\boldsymbol{n}_0}{\boldsymbol{N}_{\mathrm{all}} (1 - \varepsilon_{\mathrm{v}})} \boldsymbol{V}_{\mathrm{total}} \tag{A4}$$

$$\boldsymbol{V}_{\mathrm{total}} = (1 - \boldsymbol{x}) \left(\frac{\boldsymbol{M}_{\mathrm{ZnO}}}{\rho_{\mathrm{ZnO}}} + \frac{\boldsymbol{M}_{\mathrm{Fe2O3}}}{\rho_{\mathrm{Fe2O3}}} \right) + \boldsymbol{x} \left(\frac{\boldsymbol{M}_{\mathrm{ZnFe2O4}}}{\rho_{\mathrm{ZnFe2O4}}} \right) \tag{A5}$$

where $\boldsymbol{V}_{\mathrm{total}}$ is the total molar true volume of the granule particles at $\boldsymbol{x}$. Using Eqs. (A1), (A2), (A3), (A4), and (A5), the volume fractions ϕ_{ZnO}, ϕ_{Fe2O3}, and ϕ_{ZnFe2O4} of the nanoparticles in a single granule particle including voids are expressed by Eqs. (A6), (A7), and (A8), respectively.

$$\phi_{\mathrm{ZnO}} = \frac{\boldsymbol{V}_{\mathrm{ZnO}}}{\boldsymbol{V}_{\mathrm{g}}} = (1 - \boldsymbol{x}) \left(\frac{\boldsymbol{M}_{\mathrm{ZnO}}}{\rho_{\mathrm{ZnO}}} \right) \frac{1 - \varepsilon_{\mathrm{v}}}{\boldsymbol{V}_{\mathrm{total}}} \tag{A6}$$

$$\phi_{\mathrm{Fe2O3}} = \frac{\boldsymbol{V}_{\mathrm{Fe2O3}}}{\boldsymbol{V}_{\mathrm{g}}} = (1 - \boldsymbol{x}) \left(\frac{\boldsymbol{M}_{\mathrm{Fe2O3}}}{\rho_{\mathrm{Fe2O3}}} \right) \frac{1 - \varepsilon_{\mathrm{v}}}{\boldsymbol{V}_{\mathrm{total}}} \tag{A7}$$

$$\phi_{\mathrm{ZnFe2O4}} = \frac{\boldsymbol{V}_{\mathrm{ZnFe2O4}}}{\boldsymbol{V}_{\mathrm{g}}} = \boldsymbol{x} \left(\frac{\boldsymbol{M}_{\mathrm{ZnFe2O4}}}{\rho_{\mathrm{ZnFe2O4}}} \right) \frac{1 - \varepsilon_{\mathrm{v}}}{\boldsymbol{V}_{\mathrm{total}}} \tag{A8}$$

The nanoparticles and voids can be exposed on the surfaces of the granule particles at the same area fractions as ϕ_{ZnO}, ϕ_{Fe2O3}, and ϕ_{ZnFe2O4}, because the nanoparticles are distributed homogeneously with the voids in the granule particles as well as on their surfaces. Considering the collision pairs of the granule particles and the fraction of ZnO and Fe_2O_3

nanoparticles exposed on the surfaces of the granule particles, the collision frequency Z_{nano} between ZnO nanoparticles and Fe_2O_3 nanoparticles on the surfaces of the granule particles can be expressed as Eq. (A9) using Eqs. (A6) and (A7), and the total collision number Z_{all} of the granule particles per unit time:

$$Z_{nano} = \left\{ \frac{N_{all} P_1 \phi_{ZnO} \cdot {}_{(N_{all}-1)} P_1 \phi_{Fe2O3}}{N_{all} P_2} + \frac{N_{all} P_1 \phi_{Fe2O3} \cdot {}_{(N_{all}-1)} P_1 \phi_{ZnO}}{N_{all} P_2} \right\} Z_{all}$$

$$= \left\{ \frac{N_{all} \phi_{ZnO} \cdot (N_{all}-1) \phi_{Fe2O3}}{N_{all}(N_{all}-1)} + \frac{N_{all} \phi_{Fe2O3} \cdot (N_{all}-1) \phi_{ZnO}}{N_{all}(N_{all}-1)} \right\} Z_{all}$$

$$= 2\left(\frac{M_{ZnO} M_{Fe2O3}}{\rho_{ZnO} \rho_{Fe2O3}} \right) \frac{(1-x)^2 (1-\varepsilon_v)^2}{V_{total}^{\ 2}} Z_{all} \quad \text{(A9)}$$

where ${}_aP_b$ indicates the permutation, and a and b are positive integers ($a \geq b$).

Subsequently, the numbers N_{ZnO}, N_{Fe2O3}, and $N_{ZnFe2O4}$ of the ZnO, Fe_2O_3, and $ZnFe_2O_4$ spheres in the simulation are given by Eqs. (A10), (A11), and (A12), respectively, using the true density $\bar{\rho}$ and the volume V_g (including voids) of a single granule particle, because the spheres have the same diameter, true density, and void fraction as the granule particles:

$$N_{ZnO} = \frac{n_0 (1-x) M_{ZnO}}{\bar{\rho} V_g (1-\varepsilon_v)} \quad \text{(A10)}$$

$$N_{Fe2O3} = \frac{n_0 (1-x) M_{Fe2O3}}{\bar{\rho} V_g (1-\varepsilon_v)} \quad \text{(A11)}$$

$$N_{ZnFe2O4} = \frac{n_0 x M_{ZnFe2O4}}{\bar{\rho} V_g (1-\varepsilon_v)} \quad \text{(A12)}$$

where $n_0(1-x)M_{ZnO}$, $n_0(1-x)M_{Fe2O3}$, and $n_0 x M_{ZnFe2O4}$ are the total masses of ZnO, Fe_2O_3,

and $ZnFe_2O_4$ spheres, respectively. $\bar{\rho}\boldsymbol{V}_g(1-\varepsilon_v)$ is the mass of a single sphere, which is given by Eqs. (A13) and (A14).

$$\bar{\rho}\boldsymbol{V}_g(1-\varepsilon_v)=\frac{\boldsymbol{n}_0}{\boldsymbol{N}_{all}}\boldsymbol{W}_{total} \tag{A13}$$

$$\boldsymbol{W}_{total}=(1-\boldsymbol{x})(\boldsymbol{M}_{ZnO}+\boldsymbol{M}_{Fe2O3})+\boldsymbol{x}\boldsymbol{M}_{ZnFe2O4} \tag{A14}$$

where $\boldsymbol{W}_{total}$ is the total molar mass of the spheres at $\boldsymbol{x}$. By using Eq. (A13), Eqs. (A10), (A11), and (A12) can be rewritten as Eqs. (A15), (A16), and (A17), respectively.

$$\boldsymbol{N}_{ZnO}=\frac{\boldsymbol{N}_{all}(1-\boldsymbol{x})\boldsymbol{M}_{ZnO}}{\boldsymbol{W}_{total}} \tag{A15}$$

$$\boldsymbol{N}_{Fe2O3}=\frac{\boldsymbol{N}_{all}(1-\boldsymbol{x})\boldsymbol{M}_{Fe2O3}}{\boldsymbol{W}_{total}} \tag{A16}$$

$$\boldsymbol{N}_{ZnFe2O4}=\frac{\boldsymbol{N}_{all}\boldsymbol{x}\boldsymbol{M}_{ZnFe2O4}}{\boldsymbol{W}_{total}} \tag{A17}$$

Considering the types of collision pairs of the spheres and the voids on the surfaces of the spheres, the collision frequency $\boldsymbol{Z}_{sp}$ between ZnO spheres and Fe_2O_3 spheres is expressed as Eq. (A18) using Eqs. (A15) and (A16).

$$\boldsymbol{Z}_{sp}=\left\{\frac{\boldsymbol{N}_{ZnO}\mathrm{C}_1(1-\varepsilon_v)\cdot\boldsymbol{N}_{Fe2O3}\mathrm{C}_1(1-\varepsilon_v)}{\boldsymbol{N}_{all}\mathrm{C}_2}\right\}\boldsymbol{Z}_{all}=\left\{\frac{\boldsymbol{N}_{ZnO}\boldsymbol{N}_{Fe2O3}(1-\varepsilon_v)^2}{\boldsymbol{N}_{all}(\boldsymbol{N}_{all}-1)/2}\right\}\boldsymbol{Z}_{all}$$

$$=\frac{2(1-\boldsymbol{x})^2\boldsymbol{M}_{ZnO}\boldsymbol{M}_{Fe2O3}(1-\varepsilon_v)^2}{\boldsymbol{W}_{total}{}^2(1-1/\boldsymbol{N}_{all})}\boldsymbol{Z}_{all} \tag{A18}$$

where ${}_{\boldsymbol{a}}\mathrm{C}_{\boldsymbol{b}}$ indicates the combination, and $\boldsymbol{a}$ and $\boldsymbol{b}$ are positive integers ($\boldsymbol{a}\geq\boldsymbol{b}$). Eq. (A18) can be rewritten as Eq. (A19) because $\boldsymbol{N}_{all}$ is much larger than 1.

$$\boldsymbol{Z}_{\mathrm{sp}} = \frac{2(1-\boldsymbol{x})^2 \boldsymbol{M}_{\mathrm{ZnO}} \boldsymbol{M}_{\mathrm{Fe2O3}} (1-\varepsilon_{\mathrm{v}})^2}{\boldsymbol{W}_{\mathrm{total}}{}^2} \boldsymbol{Z}_{\mathrm{all}} \tag{A19}$$

Accordingly, by substituting Eq. (A19) into Eq. (A9), the relationship between $\boldsymbol{Z}_{\mathrm{nano}}$ and $\boldsymbol{Z}_{\mathrm{sp}}$ is obtained.

$$\boldsymbol{Z}_{\mathrm{nano}} = \frac{\boldsymbol{W}_{\mathrm{total}}{}^2}{\boldsymbol{V}_{\mathrm{total}}{}^2 \rho_{\mathrm{ZnO}} \rho_{\mathrm{Fe2O3}}} \boldsymbol{Z}_{\mathrm{sp}} \tag{A20}$$

References

[1] C. Suryanarayana, Mechanical alloying and milling, Prog. Mater. Sci. 46 (2001) 1–184, https://doi.org/10.1016/S0079-6425(99)00010-9.

[2] P. Baláž, M. Achimovičová, M. Baláž, P. Billik, Z. Cherkezova-Zheleva, J.M. Criado, F. Delogu, E. Dutková, E. Gaffet, F.J. Gotor, R. Kumar, I. Mitov, T. Rojac, M. Senna, A. Streletskii, K. Wieczorek-Ciurowa, Hallmarks of mechanochemistry: from nanoparticles to technology, Chem. Soc. Rev. 42 (2013) 7571–7637, https://doi.org/10.1039/C3CS35468G.

[3] E.L. Dreizin, M. Schoenitz, Mechanochemically prepared reactive and energetic materials: a review, J. Mater. Sci. 52 (2017) 11789–11809, https://doi.org/10.1007/s10853-017-0912-1.

[4] A.F. Fuentes, L. Takacs, Preparation of multicomponent oxides by mechanochemical methods, J. Mater. Sci. 48 (2013) 598–611, https://doi.org/10.1007/s10853-012-6909-x.

[5] V. Šepelák, I. Bergmann, S. Indris, A. Feldhoff, H. Hahn, K.D. Becker, C.P. Grey, P. Heitjans, High-resolution ^{27}Al MAS NMR spectroscopic studies of the response of spinel aluminates to mechanical action, J. Mater. Chem. 21 (2011) 8332–8337,

https://doi.org/10.1039/c0jm03721d.

[6] M. Leonardi, M. Villacampa, J.C. Menéndez, Multicomponent mechanochemical synthesis, Chem. Sci. 9 (2018) 2042–2064, https://doi.org/10.1039/c7sc05370c.

[7] L. Ouyang, Z. Cao, H. Wang, R. Hu, M. Zhu, Application of dielectric barrier discharge plasma-assisted milling in energy storage materials – a review, J. Alloys Compd. 691 (2017) 422–435, http://dx.doi.org/10.1016/j.jallcom.2016.08.179.

[8] M. Wilkening, A. Düvel, F. Preishuber-Pflügl, K. Silva, S. Breuer, V. Šepelák, P. Heitjans, Structure and ion dynamics of mechanosynthesized oxides and fluorides, Z. Kristallogr. Cryst. Mater. 232 (2017) 107–127, https://doi.org/10.1515/zkri-2016-1963.

[9] Z. Tang, S. Lim, Y. Pang, H. Ong, K. Lee, Synthesis of biomass as heterogeneous catalyst for application in biodiesel production: state of the art and fundamental review, Renew. Sust. Energ. Rev. 92 (2018) 235–253, https://doi.org/10.1016/j.rser.2018.04.056.

[10] P. Lahijani, Z.A. Zainal, M. Mohammadi, A.R. Mohamed, Conversion of the greenhouse gas CO_2 to the fuel gas CO via the Boudouard reaction: a review, Renew. Sust. Energ. Rev. 41 (2015) 615–632, http://dx.doi.org/10.1016/j.rser.2014.08.034.

[11] A. Oliva, M. Llabrés, J.B. Fariña, Data analysis in stability studies of biopharmaceutical drugs with isothermal and non-isothermal assays, Trends Anal. Chem. 30 (2011) 717–730, https://doi.org/10.1016/j.trac.2011.01.013.

[12] H. Lynggaard, A. Andreasen, C. Stegelmann, P. Stoltze, Analysis of simple kinetic models in heterogeneous catalysis, Prog. Surf. Sci. 77 (2004) 71–137, https://doi.org/10.1016/j.progsurf.2004.09.001.

[13] D.W. Ball, Physical Chemistry, 2nd ed. Cengage Learning, Boston, 2014.

[14] G.M. Barrow, Physical Chemistry, 5th ed. McGraw-Hill, New York, 1988.

[15] H. Salazar-Tamayo, M.A. Márquez, C.A. Barrero, Effect of machine variables in the

mechanosynthesis of $NiFe_2O_4$: a microstructural and kinematical study, Powder Technol. 289 (2016) 126–134, http://dx.doi.org/10.1016/j.powtec.2015.11.056.

[16] G. Cagnetta, J. Huang, B. Wang, S. Deng, G. Yu, A comprehensive kinetic model for mechanochemical destruction of persistent organic pollutants, Chem. Eng. J. 291 (2016) 30–38, http://dx.doi.org/10.1016/j.cej.2016.01.079.

[17] F. Delogu, L. Takacs, Information on the mechanism of mechanochemical reaction from detailed studies of the reaction kinetics, J. Mater. Sci. 53 (2018) 13331–13342, https://doi.org/10.1007/s10853-018-2090-1.

[18] Z. Chen, S. Lu, Q. Mao, A. Buekens, Y. Wang, J. Yan, Energy transfer and kinetics in mechanochemistry, Environ. Sci. Pollut. Res. 24 (2017) 24562–24571, https://doi.org/10.1007/s11356-017-0028-9.

[19] G. Lee, E. Park, S. Yang, J. Park, S. Bu, M. Lee, Rapid and direct synthesis of complex perovskite oxides through a highly energetic planetary milling, Sci. Rep. 7 (2017), 46241. https://doi.org/10.1038/srep46241.

[20] P.A. Cundall, O.D.L. Strack, A discrete numerical model for granular assemblies, Géotechnique 29 (1979) 47–65.

[21] L.M. Tavares, A review of advanced ball mill modelling, KONA Powder Part. J. 34 (2017) 106–124, https://doi.org/10.14356/kona.2017015.

[22] J. Tang, J. Qiao, Z. Liu, X. Zhou, G. Yu, J. Zhao, Mechanism characteristic analysis and soft measuring method review for ball mill load based on mechanical vibration and acoustic signals in the grinding process, Min. Eng. 128 (2018) 294–311, https://doi.org/10.1016/j.mineng.2018.09.006.

[23] C.M.R. Mudiyanselage, H.C.P. Karunasena, Y.T. Gu, L. Guan, W. Senadeera, Novel trends in numerical modelling of plant food tissues and their morphological changes

during drying – a review, J. Food Eng. 194 (2017) 24–39, http://dx.doi.org/10.1016/j.jfoodeng.2016.09.002.

[24] J. Horabik, M. Molenda, Parameters and contact models for DEM simulations of agricultural granular materials: a review, Biosyst. Eng. 147 (2016) 206–225, http://dx.doi.org/10.1016/j.biosystemseng.2016.02.017.

[25] Y. Tsuji, T. Tanaka, T. Ishida, Lagrangian numerical simulation of plug flow of cohesionless particles in a horizontal pipe, Powder Technol. 71 (1992) 239–250, https://doi.org/10.1016/0032-5910(92)88030-L.

[26] W.D. Callister, Jr., D.G. Rethwisch, Materials Science and Engineering: An Introduction, 8th ed. John Wiley & Sons, New Jersey, 2009.

[27] A.G.E. Sutjipto, M.H. Mazwir, H.L. Yee, S.R. Misskon, A.G.M. Shaitir, M.A. Jusoh, R. Othman, Effect of compaction pressure of green body and heating current on photoluminescence property of ZnO crystal grown by electric current heating method, IOP Conf. Ser. 290 (2018), 012043. https://doi.org/10.1088/1757-899X/290/1/012043.

[28] M. Zdujić, Č. Jovalekić, L. Karanović, M. Mitrić, D. Poleti, D. Skala, Mechanochemical treatment of α-Fe_2O_3 powder in air atmosphere, Mater. Sci. Eng. A 245 (1998) 109–117, https://doi.org/10.1016/S0921-5093(97)00715-6.

[29] H. Ling, A. Petric, Electrical and thermal properties of spinels, Proc. Electrochem. Soc. PV 2005-07 (2005) 1866–1873.

[30] H.N. Yoshimura, A.L. Molisani, N.E. Narita, J.L.A. Manholetti, J.M. Cavenaghi, Mechanical properties and microstructure of zinc oxide varistor ceramics, Mater. Sci. Forum 530, 531 (2006) 408–413, https://doi.org/10.4028/www.scientific.net/MSF.530-531.408.

[31] L. Oravova, Z. Zhang, N. Church, R.J. Harrison, C.J. Howard, M.A. Carpenter,

Elastic and anelastic relaxations accompanying magnetic ordering and spin-flop transitions in hematite, Fe_2O_3, J. Phys. Condens. Matter 25 (2013), 116006. https://doi.org/10.1088/0953-8984/25/11/116006.

[32] T.R. Tatarchuk, N.D. Paliychuk, M. Bououdina, B. Al-Najar, M. Pacia, W. Macyk, A. Shyichuk, Effect of cobalt substitution on structural, elastic, magnetic and optical properties of zinc ferrite nanoparticles, J. Alloys Compd. 731 (2018) 1256–1266, https://doi.org/10.1016/j.jallcom.2017.10.103.

[33] A.W. Bruno, D. Gallipoli, C. Perlot, J. Mendes, Mechanical behaviour of hypercompacted earth for building construction, Mater. Struct. 50 (2017) 160, https://doi.org/10.1617/s11527-017-1027-5.

[34] T. Suzuki, M. Ohtsu, M. Shigeishi, Relative damage evaluation of concrete in a road bridge by AE rate-process analysis, Mater. Struct. 40 (2007) 221–227, https://doi.org/10.1617/s11527-006-9133-9.

[35] Y. Konishi, K. Kadota, Y. Tozuka, A. Shimosaka, Y. Shirakawa, Amorphization and radical formation of cystine particles by a mechanochemical process analyzed using DEM simulation, Powder Technol. 301 (2016) 220–227, http://dx.doi.org/10.1016/j.powtec.2016.06.010.

[36] T. Iwasaki, Novel mechanochemical process for aqueous-phase synthesis of superparamagnetic magnetite nanoparticles, in: S. Hutagalung (Ed.), Materials Science and Technology, In Tech, London 2012, pp. 235–256.

[37] W. Kim, F. Saito, Mechanochemical synthesis of zinc ferrite from zinc oxide and α-Fe_2O_3, Powder Technol. 114 (2001) 12–16, https://doi.org/10.1016/S0032-5910(00)00256-4.

Table 1
Parameters used in the simulation.

Number:	
Balls	180
Granule particles	2862
Ball/granule particle filling mass ratio	28.3
Ball/granule particle filling volume ratio	18.6
Diameter:	
Balls	5.0 mm
Granule particles	0.75 mm
Density:	
Balls	6000 kg/m^3 [26]
Granule particles	3955 kg/m^3 [27–29]
Poisson's ratio:	
Balls, wall	0.31 [26]
Granule particles	0.32 [30–32]
Young's modulus:	
Balls, wall	205 GPa [26]
Granule particles	18.6 GPa [30–34]
Coefficient of restitution:	
Ball-to-ball, ball-to-wall	0.84
Granule particle-to-ball, granule particle-to-wall	0.68
Granule particle-to-granule particle	0.55
Friction coefficient:	
Ball-to-ball, ball-to-wall	0.53
Granule particle-to-ball, granule particle-to-wall	0.55
Granule particle-to-granule particle	0.60
Pot volume	45 mL
Pot diameter	40 mm
Pot depth	35.8 mm
Revolution speed	5.0–10.0 s^{-1}
Revolution radius	67 mm
Rotation-to-revolution speed ratio	–1
Time step	100 ns

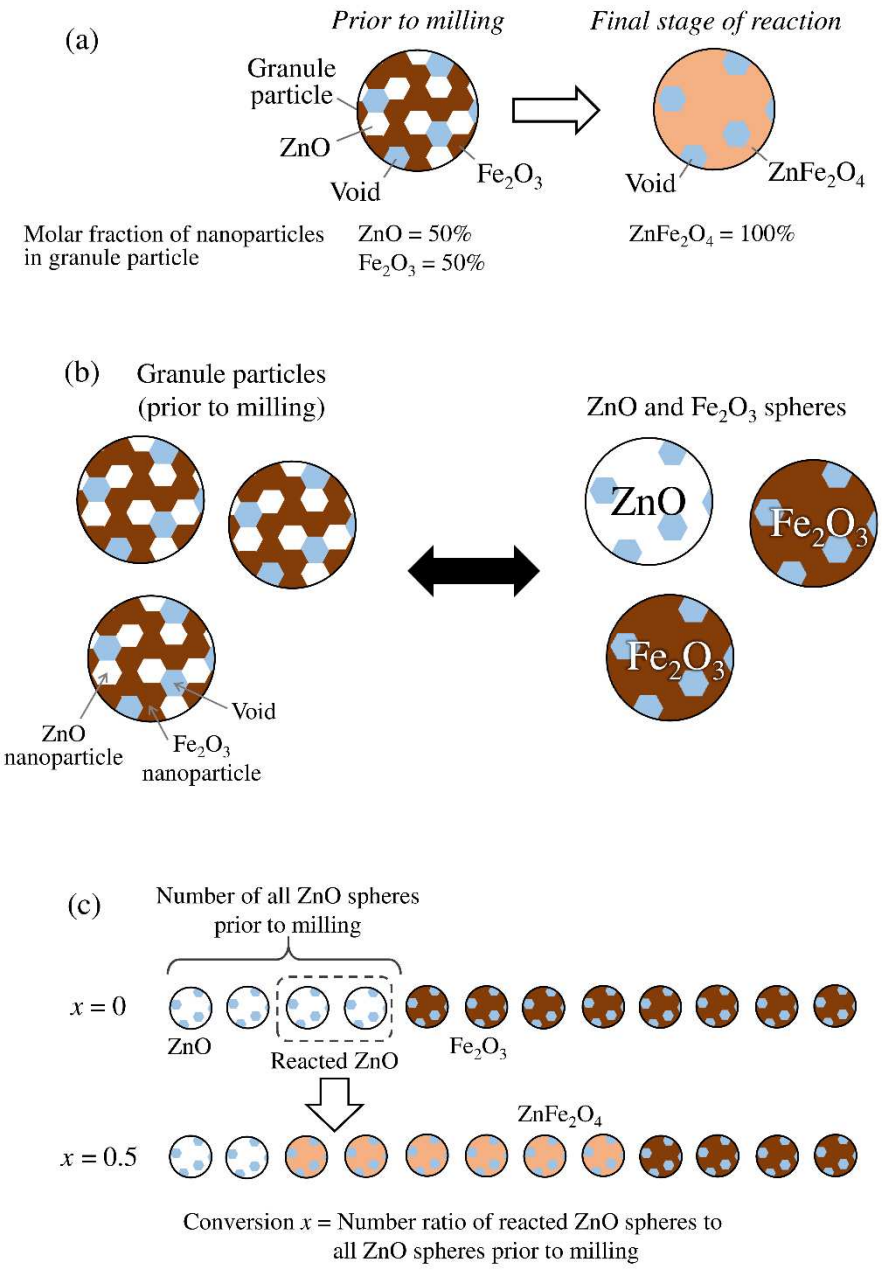

Fig. 1. Definition of the (a) granule particles, (b) spheres, and (c) the conversion ***x*** used in the simulation.

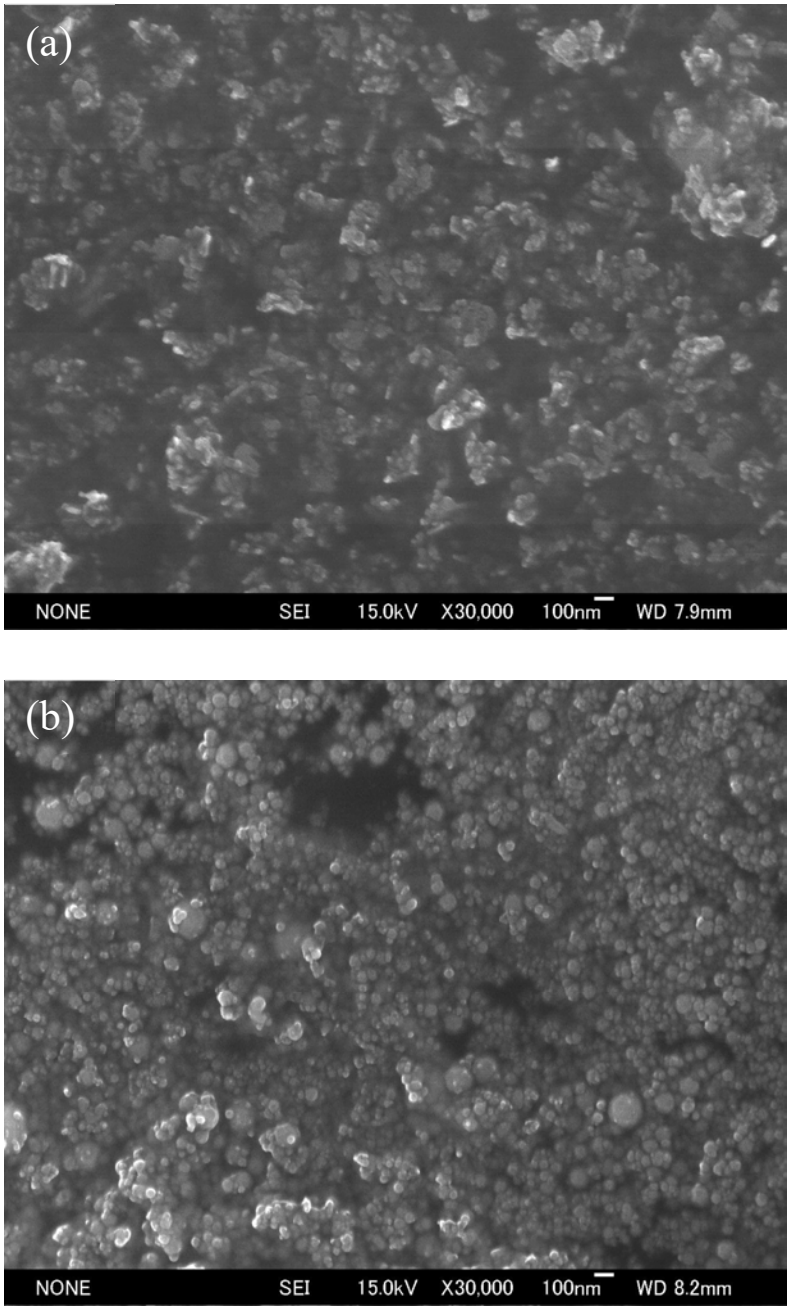

Fig. 2. Typical SEM images of (a) ZnO and (b) γ-Fe_2O_3 nanoparticles.

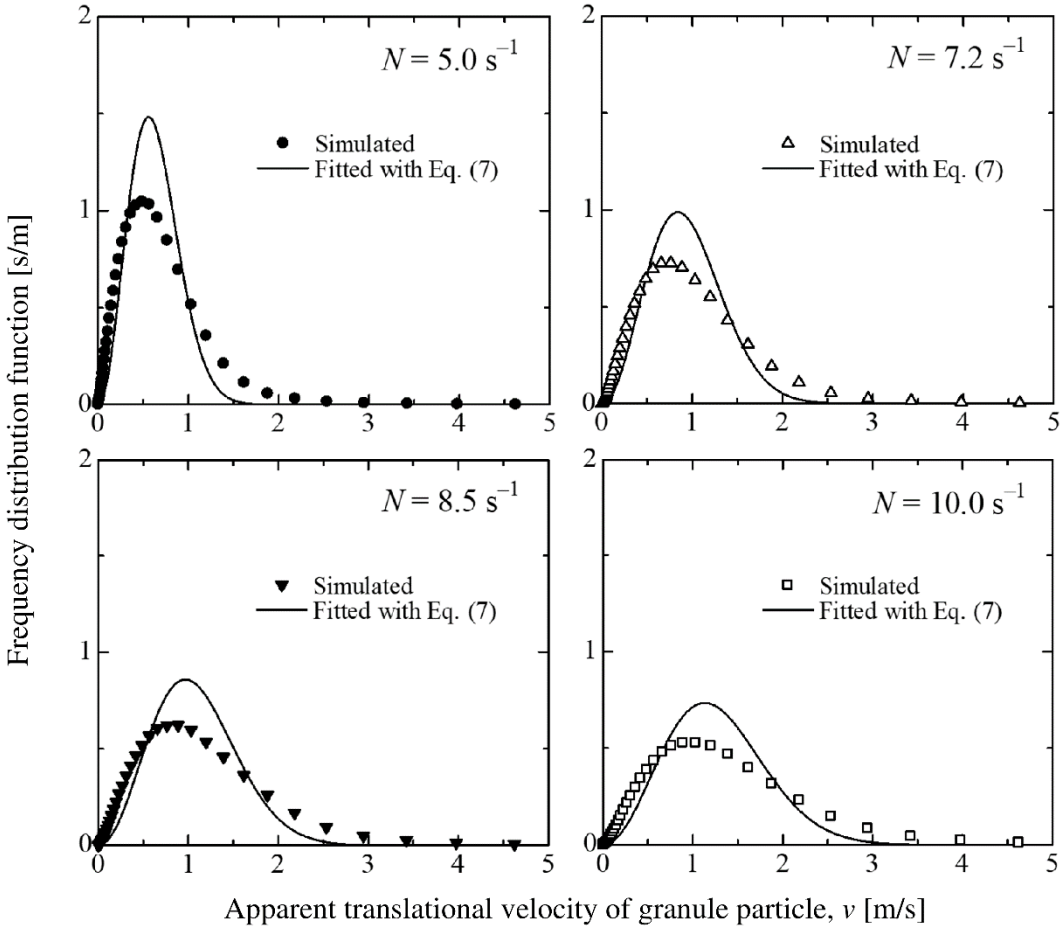

Fig. 3. Apparent translational velocity distributions of the granule particles.

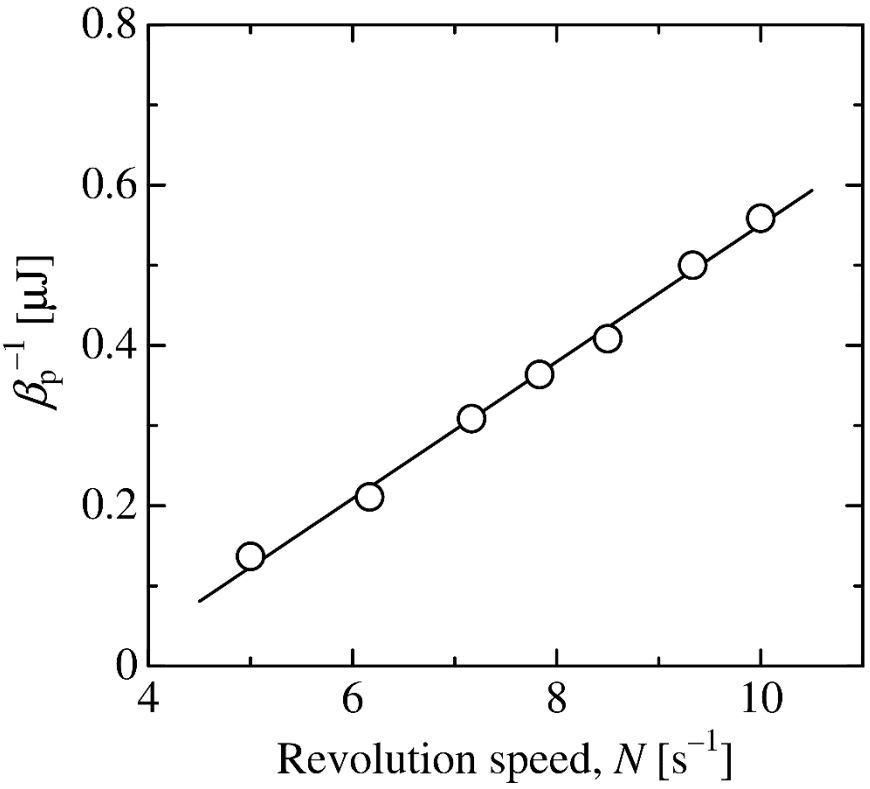

Fig. 4. Change in $1/\beta_p$ of the granule particles with revolution speed.

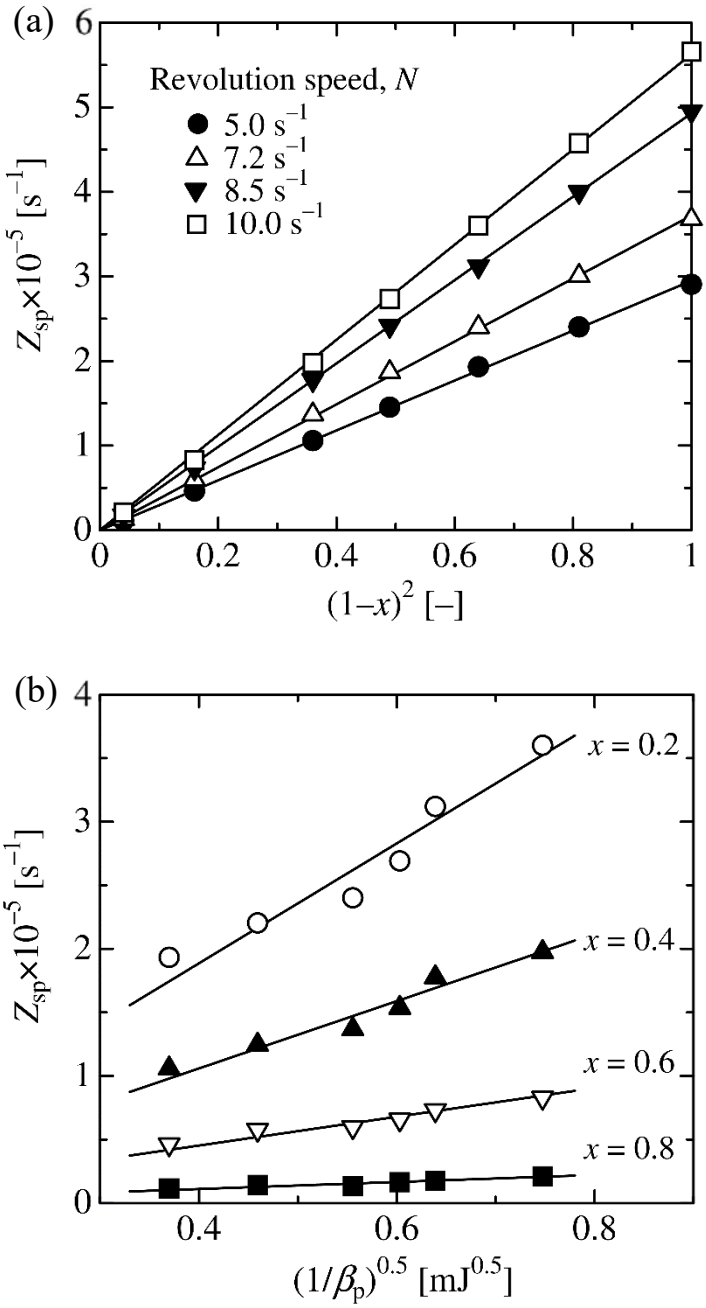

Fig. 5. Relationships (a) between Z_{sp} and $(1–x)^2$ and (b) between Z_{sp} and $(1/\beta_p)^{0.5}$.

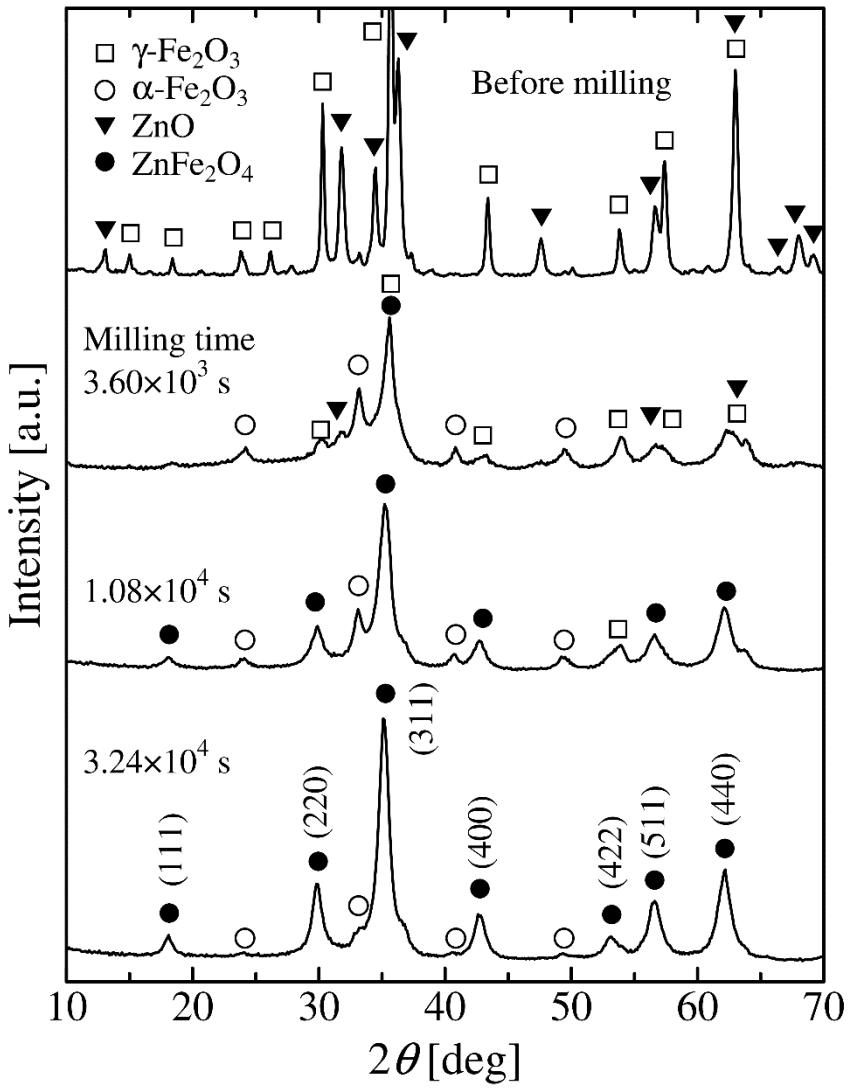

Fig. 6. Effect of milling time on the phase evolution of $ZnFe_2O_4$ during milling at 10.0 s^{-1}.

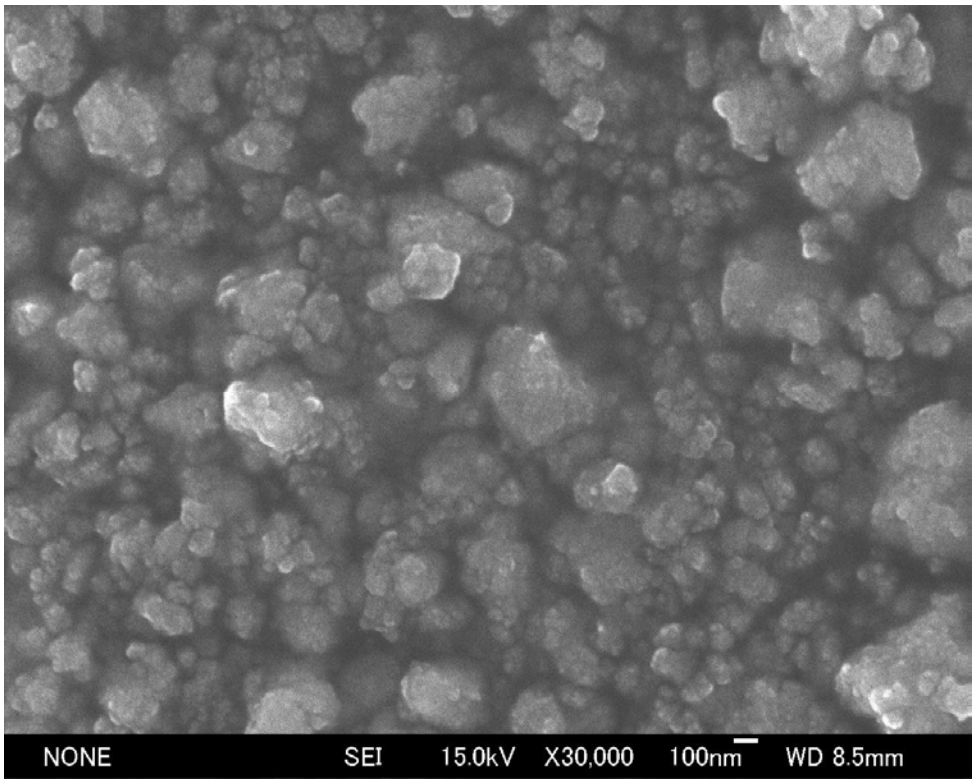

Fig. 7. Typical SEM image of sample obtained after milling for 3.24×10^4 s at $\boldsymbol{N} = 10.0$ s^{-1}.

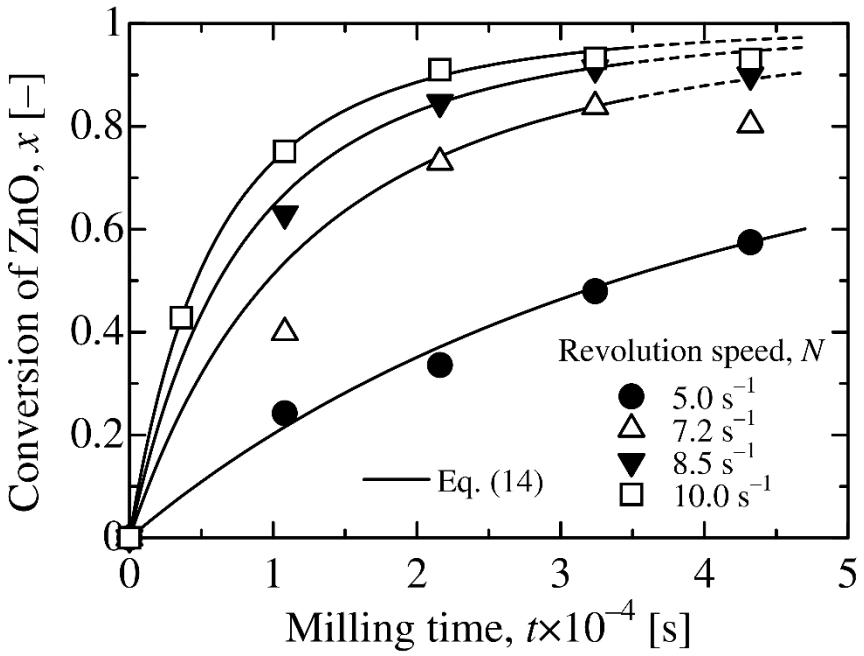

Fig. 8. Change in the conversion of ZnO with milling time at different revolution speeds.

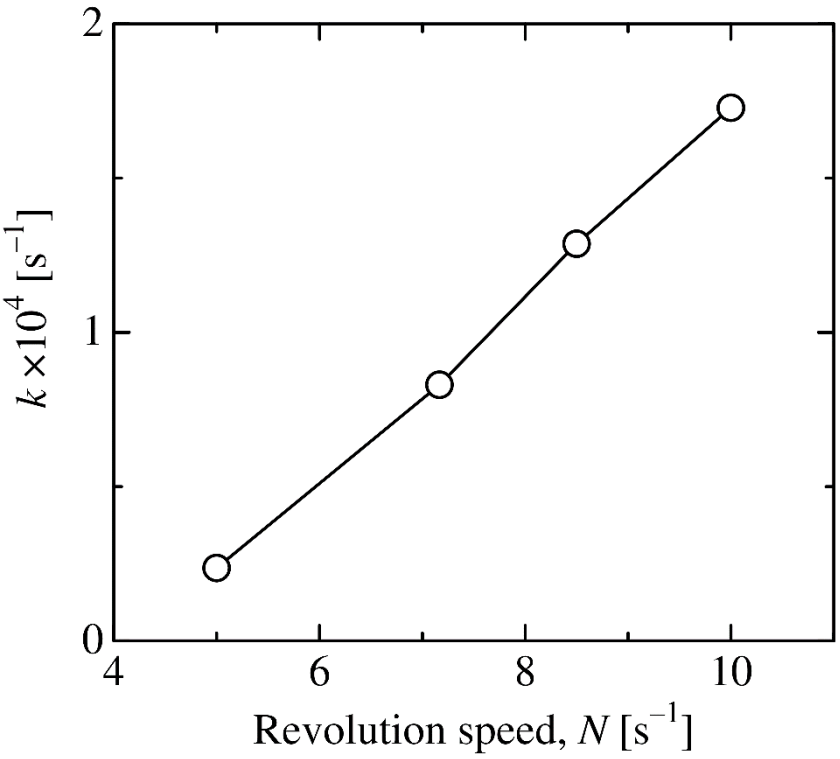

Fig. 9. Change in the reaction rate constant ***k*** with revolution speed.

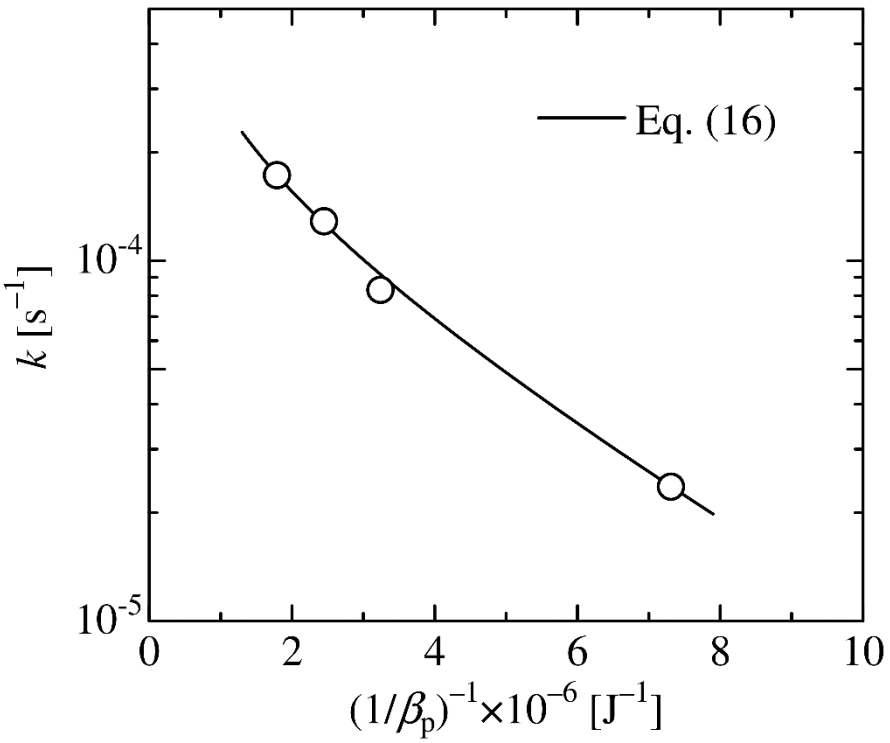

Fig. 10. Relationship between ***k*** and $1/\beta_p$.